Hindawi
Scientific Programming
Volume 2022, Article ID 4154660, 9 pages
https://doi.org/10.1155/2022/4154660

Research Article

Classification and Recognition of Doppler Ultrasound Images of Patients with Atrial Fibrillation under Machine Learning

Xiaoyuan Wang, Meiling Du, Aiai Zhang, Feixing Li, Mengyang Yi, and Fangjiang Li

Department of Cardiovascular Medicine, The First Affiliated Hospital of Hebei North University, Zhangjiakou 075000, Hebei, China

Correspondence should be addressed to Xiaoyuan Wang; wangxiaoyuan@hebeinu.edu.cn

Received 23 November 2021; Accepted 13 January 2022; Published 11 March 2022

Academic Editor: M Pallikonda Rajasekaran

This study was aimed to explore the value of the twin neural network model in the classification and recognition of cardiac ultrasound images of patients with atrial fibrillation. 80 patients with cardiac atrial fibrillation were selected and randomly divided into experimental group (40 cases) and control group (40 cases). The twin neural network (TNN) model was combined with traditional ultrasound, Doppler spectrum, tissue velocity, and strain imaging technology to obtain the patient's cardiac structure parameters and analyze and compare related indicators. The results showed that the total atrial emptying fraction (TA-EF value) of the experimental group was 53.08%, which was significantly lower than that of the control group ($P < 0.05$). There were no significant differences in left atrial diameter (LAD), left ventricular end-diastolic diameter (LVEDD), left atrial maximum volume (LAVmax), and left ventricular ejection fraction (LVEF) between the two groups. In the experimental group, the average peak velocity of mitral valve annulus (Em) was 8.49 cm/s, the peak velocity of lateral wall systole (Vs) was 6.82 cm/s, and the propagation velocity of left ventricular blood flow (Vp) was 51.2 cm/s, which were significantly reduced ($P < 0.05$). The average values of peak strains in the middle and upper left atrium of the experimental group were significantly lower than those of the control group ($P < 0.05$). It can be concluded that the combined use of the TNN model can more accurately and quickly classify and recognize ultrasound images.

1. Introduction

Cardiac atrial fibrillation is one of the most common clinical arrhythmias, which is also known as atrial fibrillation. Epidemiological surveys show that the incidence of atrial fibrillation in the population is 0.4%–1%, and it continues to increase with age [1]. Based on the Studies of Left Ventricular Dysfunction (SOLVD), it is found that the mortality rate of patients with atrial fibrillation is about 34%, while the mortality rate of patients with sinus rhythm is about 23%. The main reason for this difference is that the patient is accompanied with congestive heart failure rather than thromboembolism [2, 3]. Many heart failure experiments have shown that atrial fibrillation is a very good independent predictor for predicting the incidence of heart failure and death caused by it. Heart failure can cause atrial fibrillation, and atrial fibrillation can aggravate heart failure. The two affect each other, and the patient's prognosis is poor. Therefore, it has controlled heart failure to treat the atrial fibrillation, and the effective control of atrial fibrillation is an important part of treating heart failure, which means that it is particularly important to accurately assess the heart function level of patients with atrial fibrillation [4, 5]. Studies have shown that the heart failure function classification proposed by the New York Heart Association (NYHA) is not sensitive to the assessment of the quality of life of patients with atrial fibrillation [6]. In clinical practice, traditional cardiac ultrasound images are used to evaluate the cardiac function of patients with atrial fibrillation. For example, the systolic function of the left ventricle is evaluated using the

shortening rate of the short axis of the left ventricle and the ejection fraction of the left ventricle; the diastolic function of the left ventricle is evaluated by the diastolic period of the mitral valve orifice and the blood flow spectrum of the pulmonary vein; and the left atrial function is evaluated using the active ejection fraction of the left atrium, the volume of the left atrium, and the ejection force of the left atrium [7, 8].

Cardiac ultrasound images obtain the periodic activity information of heart tissue structures (such as myocardium, intracardiac, adventitia, and ventricles). It uses the unique physical properties of ultrasound to accurately describe the movement of the myocardium by drawing active images of the heart tissue structure. It has received widespread attention in the clinical diagnosis and treatment of various heart diseases, and has become the most commonly used imaging method for the diagnosis and treatment of patients with heart diseases [9]. As one of the characteristics of cardiac ultrasound images, speckle not only represents noise but also represents a lot of tissue structure information so as to express the physical characteristics of the heart tissue structure. In addition, the position of the speckle is relatively stable, and it can be used to track the speckle characteristics in adjacent frames to obtain the displacement parameter of any point in the myocardium [10]. According to the uniqueness and stability of speckles, echocardiographic speckle tracking technology (STE) can automatically identify and track the spatial movement of speckles to obtain myocardial velocity, displacement, and deformation parameters, thereby calculating myocardial strain and strain rate. Therefore, it is of great significance in the evaluation of many heart diseases [11]. Using speckle to distribute features in an image and then manually processing is the main working mode of traditional STE. For example, tracking the specified position in two frames of images is achieved by two-dimensional (2D) STE using speckle features in the block matching method. However, traditional STE is time consuming and labor intensive in tracking accuracy and tracking speed, and it can be improved greatly [12].

In recent years, half of the applications in the target tracking field are occupied by the twin neural network (TNN) due to the rapid development of deep learning technology. It can realize single-sample learning, which makes it unique advantages in image block matching. The application of TNN to target tracking can ensure the accuracy, and it can quickly and accurately match the target, simplify the model, and improve the tracking speed [13]. TNN contains two identical network models, taking two samples as input and characteristic high-latitude space as output to compare the similarities between the two. TNN is used in target tracking, face, fingerprint recognition, etc., and has achieved outstanding results in target tracking fields such as autonomous driving and drones [14, 15]. Many experimental data have confirmed that the twin network has significant advantages in image block matching of real life scenes such as faces, roads, and animals. It not only has very high accuracy but also guarantees a considerable speed. Although there are so many speckles in the echocardiogram and the true contour of the heart in the echocardiogram is disturbed, it contains a wealth of important information such as myocardium and blood [16]. Therefore, the TNN target tracking model was combined with Doppler spectrum, tissue velocity imaging, and strain imaging to evaluate its value in the classification and recognition of echocardiography in patients with atrial fibrillation, aiming to provide theoretical basis for diagnosis and treatment of atrial fibrillation.

2. Materials and Methods

2.1. General Data. In this study, 80 patients with cardiac atrial fibrillation admitted to the hospital from May 2017 to May 2020 were selected as the research objects. According to the random number table method, 40 patients were included in the experimental group, of which 30 were patients with paroxysmal atrial fibrillation, 7 were patients with persistent atrial fibrillation, and 3 were patients with chronic atrial fibrillation; atrial fibrillation occurred in all patients with a ventricular rate of 40–100 beats per minute. Another 40 patients served as a control group. The patients and their families in this study had fully understood the situation and signed the informed consent forms. This study was approved by the ethics committee of hospital.

The inclusion criteria were referred to the Atrial Fibrillation Diagnosis and Classification Criteria in the Guidelines for the Management of Atrial Fibrillation revised by the American Heart Association (AHA) and the American College of Cardiology (ACC) in 2006 combined with the classification criteria for atrial fibrillation given by the Expert Consensus Centers of Heart Rhythm Society (HRS), the European Heart Rhythm Association (EHRA), and the European Cardiac Arrhythmia Society (ECA). All patients with atrial fibrillation had been confirmed by electrocardiograph records. Paroxysmal atrial fibrillation refers to recurrent atrial fibrillation that can be terminated spontaneously; persistent atrial fibrillation refers to the occurrence of atrial fibrillation for more than 7 days; and chronic atrial fibrillation refers to the occurrence of atrial fibrillation for more than 1 year.

Exclusion criteria were given as follows: patients with no history of cardiomyopathy, acute myocardial infarction, valvular heart disease, pulmonary heart disease, congenital heart disease, hyperthyroidism, pre-excitation syndrome, severe liver and kidney dysfunction, chest deformity, etc.; patients whose routine ultrasound showed that the heart was significantly enlarged (that was, the left ventricular end diastolic diameter (LVEDD) was less than 60 mm and the left ventricular systolic function was significantly reduced (that was, the left ventricular ejection fraction (LVEF) was greater than 45%); and patients with severe valve disease or segmental abnormalities of ventricular wall motion. The general conditions of the two groups of patients are shown in Table 1.

Comparison showed that the data of gender, average age, number of patients with hypertension, and number of patients with coronary heart disease (CHD) between the two groups were not statistically significant ($P > 0.05$).

Table 1: General conditions of the two groups of patients.

Group	Number of patients	Gender ratio	Average age	Number of patients with hypertension	Number of patients with CHD
Experimental group	40 cases	Males/females = 24 : 16	61.71 ± 15.34 years old	18 cases	22 cases
Control group	40 cases	Males/females = 22 : 18	59.62 ± 9.79 years old	17 cases	23 cases

Note. "CHD" in the table referred to coronary heart disease.

2.2. Image Acquisition and Processing Method. All patients received routine cardiac ultrasound within one day, and only took coronary dilatation and antihypertensive drugs for the first half of the year, and did not regularly take antiarrhythmic drugs. When the ultrasound examination was performed, patients were instructed to breathe calmly, lie on the left side of the examination table, connect to the electrocardiogram, and perform routine echocardiography. Based on the parasternal long-axis view of the left ventricle, the left atrial diameter (LAD) at the end of the left ventricular systole and the LVEDD at the end of the left ventricle were measured and obtained. The two-plane Simpson method was used to obtain the apical four-chamber and two-chamber views, and the left ventricular end diastolic volume (LVEVD) and left ventricular end systolic volume (LVEVS) were used to calculate the LVEF ((LVEVD–LVEVS)/LVEVD × 100%). The maximum left atrial volume (LAVmax) and the minimum left atrial volume (LAVmin) were adopted to calculate the total atrial emptying fraction (TAEF) ((LAVmax – LAVmin)/LAVmax × 100%). The blood flow spectrum of the mitral valve orifice in the apical four-chamber view was obtained to measure the peak velocity of the mitral valve in the early diastole (E), and the left ventricular blood flow velocity (VP) in the early diastole was detected. The peak velocity of the mitral valve annulus in the early diastole of each part was detected by tissue velocity imaging (TVI), the overall velocity of the movement was taken as Em, the strain image analysis and postprocessing software were adopted to measure the peak strain of the interatrial septum ($\varepsilon 1$) and the peak strain of the left atrium wall ($\varepsilon 2$), and then the mean value between the two (εm) was calculated. In addition, the TNN model was applied to classify and recognize the images so as to evaluate the cardiac function level of patients.

2.3. TNN Target Tracking Model. The siamese instance search for tracking (SINT) model contains two identical branches: query stream and search stream. They have the same network structure and parameters, and the Query stream is responsible for the input of the template image, while the Search stream is responsible for the input of the search image. The two inputs are independent of each other and do not interfere with each other. The main function of the template image is to obtain the target to be tracked by the plan, and the main function of the search image is to generate a candidate frame, which contains the target. After entering the search branch, it can use conv and maxpool to extract features and eliminate interference, respectively. When target deformation or environmental noise occurs, maxpool is used to deal with the bad effects on the tracking results and then generate many candidate boxes to determine which candidate box is the tracking target located in. Because there are too many candidate frames and they overlap each other, a lot of useless calculations are performed. Therefore, the candidate frames are transported to roipool for "pooling." This layer can increase the calculation speed by converting the feature map to a fixed length. After the region of interest (ROI) was "pooled," it could select the candidate frame that best matched the initial target using

$$\widehat{x}_n = \arg_{x_{zn}} \max h\left(x_{n=0}, x_{z,n}\right). \tag{1}$$

In the above equation, $\widehat{x}_n$ referred to the most suitable candidate frame in the n-th frame, which was the final version of the predicted target frame; $x_{z,n}$ was all the candidate frames in the n-th frame, and h represented the matching function obtained by training, as shown in the following formula:

$$h(x, y) = f(x)^N f(y). \tag{2}$$

As the depth of the model increased, the overall target can be better identified, but the identification of the details of the target was reduced. SINT used a multilayer fusion structure to fuse low-level and high-level features, and inputted them into the loss function after L2 regularization to track the target more accurately. The model used a contrastive loss function:

$$l\left(x_z, x_k, y_{zk}\right) = \frac{1}{2} y_{zk} D^2 + \frac{1}{2}\left(1 - y_{zk}\right)\max\left(0, \varepsilon - D^2\right). \tag{3}$$

Here, $y_{zk} \in \{0, 1\}$ represented whether x_z and x_k were the same object. If they were the same object, the result was 1, or otherwise, the result was 0; ε represented the minimum distance that different objects should reach; D represented the Euclidean distance represented by the L2 regularization output vector of the two branches, as shown in the following formula:

$$D = \left\| f\left(x_z\right) - f\left(x_k\right) \right\|_2. \tag{4}$$

SINT converted the basic network visual geometry group (VGG) to AlexNet with a smaller number of layers to implement comparative experiments and observed that the use of deep neural networks can significantly improve the tracking performance. At the same time, in a neural network with a smaller depth, maxpool would cause bad interference to the tracking results. SINT innovatively proposed using

TNN to implement target tracking and achieved gratifying results, which opened up a new route for the application of deep learning in target tracking.

SiamFC also had two branches, input template image and search image, respectively, and the two extracted features by using the full convolutional neural network (FCN) of the AlexNet architecture to generate feature maps. Then, the fully connected layer of AlexNet was converted to CNN, which was called FCN constructed by AlexNet, and input the two feature maps into the cross-correlation layer and performed cross-correlation operations, as shown in the following formula:

$$f(j, x) = \phi(j) * \phi(x) + b. \tag{5}$$

Here, j was the template image, x was the search image, $*$ was the convolution operation, b $\in J^2$ referred to the signal value corresponding to each position in the response graph, and f (j, x) represented the similarity of each corresponding area in the imaged j and x.

The response graph obtained by this operation still needed to be processed with a cosine window to punish large displacements. Then, the point with the highest score was selected, and the corresponding part of the point in the image was just the target to be tracked. In order to obtain the same resolution as the original image, the response map was mapped back to the original image through bitrilinear interpolation.

The input of the sample image required not only the target to be identified but also the surrounding environment information and filling. When the size of the original image cannot meet the requirements, the average value of the red-green-blue (RGB) channels was used to fill the target area to meet the required size. The background information can also be added by filling, and the model can better distinguish the target and the background. In addition, the filling maintained the integrity of the object in the sample image, and the processed target area was similar to GOTURN, which can expand the area around the target. Taking the template image as an example, the new target area obtained after expansion satisfied

$$r(v + 2p) \times r(g + 2p) = A. \tag{6}$$

Here, A was the area of the new target part and the template image. p = ((v + g)/4) was to add p units to the boundary of the target area, and r was the scale transformation from the target part to the new target part. Although the area of the new target part after the scale transformation met the requirements of the template image, the width and height did not necessarily meet the requirements. Therefore, it was necessary to fill in the insufficient area and then zoom and resize the filled image. The search image had the same principle, but the area was different. SiamFC also used multiscale feature fusion technology to have multiscale adaptability.

The loss function used by the SiamFC model was logistic loss, as shown in the following formula:

$$L(y, w) = \frac{1}{D} \sum_{o \in D} l(y[o], w[o]). \tag{7}$$

Here, w was the predicted score, $y \in \{+1, -1\}$ was the true value label, D referred to the response graph, and o $\in D$ represented a point in the response graph. L was the loss value at a certain point in the response graph, as shown in the following formula:

$$l(y, w) = \log(1 + \exp(-yw)). \tag{8}$$

The label y was as

$$y[o] = \begin{cases} +1, & \text{if } k\|o - c\| \le S, \\ -1, & \text{otherwise.} \end{cases} \tag{9}$$

Here, k was the step size and the multiple that was reduced after the model was processed. c was the center of the target, o was a point in the response graph, and S was the defined radius, and the point within the radius was the true value.

SiamFC was a representative model following SINT, which significantly enhanced the real-time performance of deep learning trackers. Afterwards, a large number of deep learning trackers were optimized on this basis.

2.4. Statistical Methods. All data were analyzed with SPSS20.0 statistical software, measurement data were expressed by $\overline{x} \pm s$, independent sample t test was used to compare the means between two groups, χ^2 test was used to compare count data, and exact probability was used when the theoretical frequency was less than 5. $P < 0.05$ indicated that the difference was statistically significant.

3. Results

3.1. Comparison on Clinical Data. The clinical characteristics of some patients with cardiac ultrasound images in the experimental group and control group are shown in Figures 1–3.

As illustrated in Figures 1–3, the patient's heart was significantly enlarged (that was, the LVEDD was less than 60 mm), and the left ventricular systolic function was greatly reduced (that was, the LVEF was greater than 45%); the disease spectrum, blood pressure, and ventricular rate showed no statistically obvious differences ($P > 0.05$).

3.2. Comparison on Ultrasound Indicators. The ultrasound indicators of patients in the experimental group and the control group are shown in Figures 4 and 5.

As shown in Figures 4 and 5, the TA-EF value of the experimental group was obviously lower than that of the control group ($P < 0.05$), and there was no visible difference in LAD, LVEDD, LAVmax, and LVEF between the two groups ($P > 0.05$).

3.3. Comparison on Blood Flow Spectrum and TVI Measurement Value. The blood flow spectrum and TVI

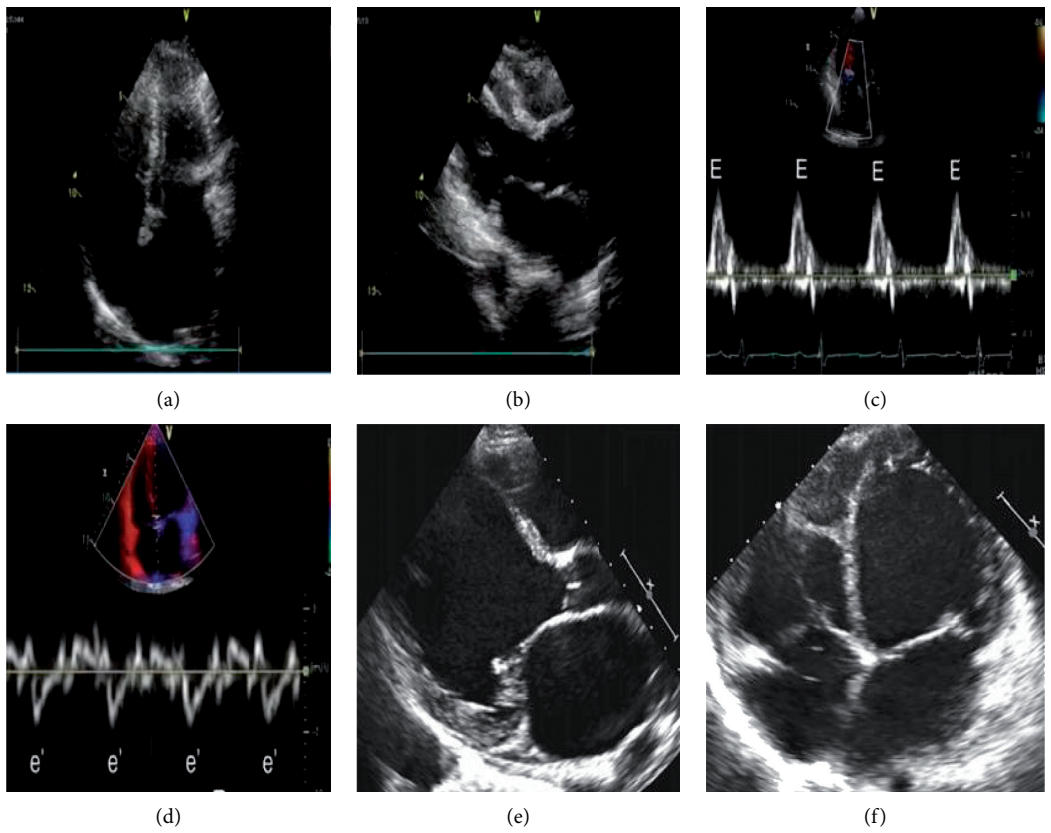

Figure 1: Partial ultrasound images of patients. Figures (a–d) are ultrasound images of patients with atrial fibrillation, E and e'peak refer to the flow velocity of the mitral valve in the early diastole, Figures (e, f) are ultrasound images of patients with atrial fibrillation and heart failure.

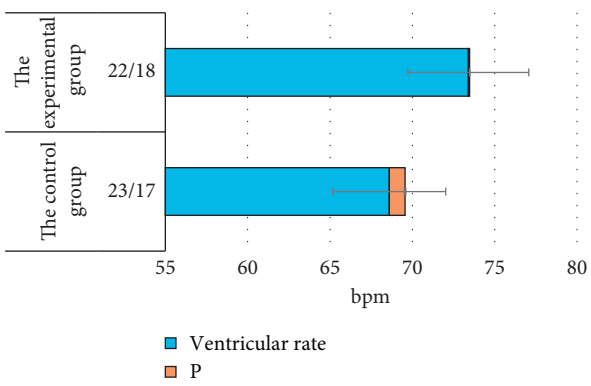

Figure 2: Comparison on disease spectrum (CHD/hypertension) and ventricular rate between the two groups.

measurement values of patients in the experimental group and the control group are shown in Figures 6 and 7.

As revealed in Figures 6 and 7, compared with the control group, the Em, Vs, and Vp values of the experimental group were significantly smaller, while the E/Em value was obviously larger ($P < 0.05$).

3.4. Comparison on Strain Imaging. The strain imaging indexes of the experimental group and the control group showed poor stability and reproducibility of the strain curve of the lower left atrium, and the peak strain was close to the baseline. Therefore, the indicators of the lower left atrium were removed, and the indicators of the upper and middle left atrium were compared, as shown in Figures 8 and 9.

As illustrated in Figures 8 and 9, the peak strain of the upper left atrium of the two groups of patients was significantly greater than that of the middle. Comparison between the two groups revealed the average value of the peak strain of the middle and upper left atrium of the experimental group was significantly smaller than that of the control group ($P < 0.05$), and the difference was statistically significant.

4. Discussion

CNN includes many categories, among which the fully convolutional TNN can effectively improve the tracking effect and speed of cardiac ultrasound, and meet the real-time requirements. However, when facing different targets, the depth of the network used to extract the target features is fixed, which makes the amount of calculation relatively large; the effect is poor when the facing target has a large change. SiamFC-based CFNet not only combines CF and depth features but also enables end-to-end training in CNN, but it cannot handle the boundary effect of the CF layer [17]. Based on the improvement of SiamFC, SiamFC++ adds the bounding box regression branch and the quality estimation

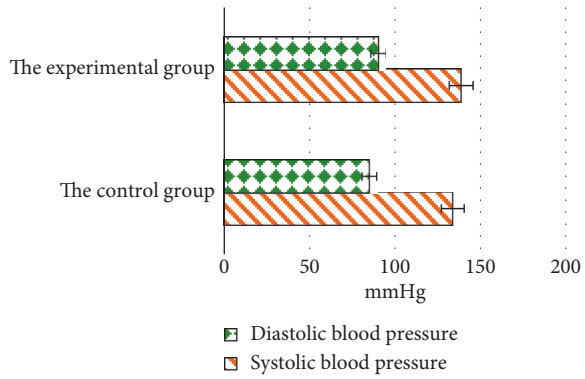

Figure 3: Comparison on systolic and diastolic blood pressure between the two groups.

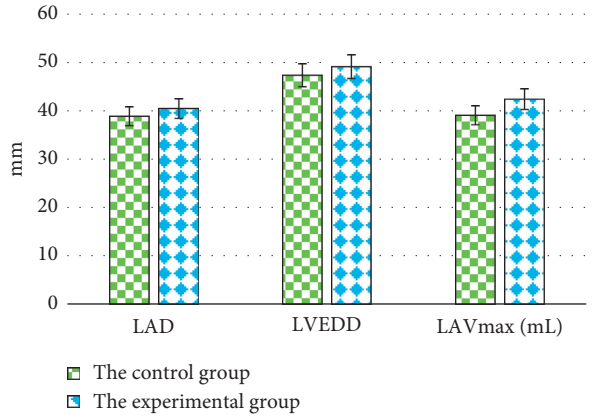

Figure 4: Comparison on LAD, LVEDD, and LAVmax between the two groups of patients.

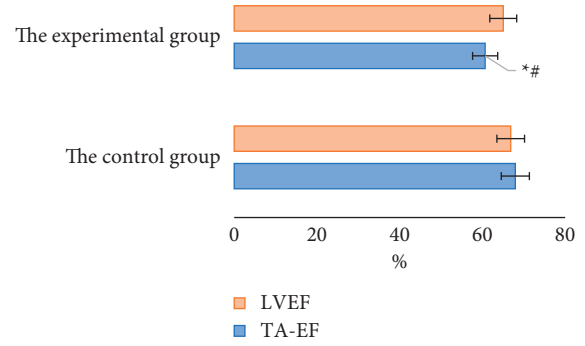

Figure 5: Comparison on TA-EF and LVEF between the two groups of patients. ∗# indicates $P < 0.05$.

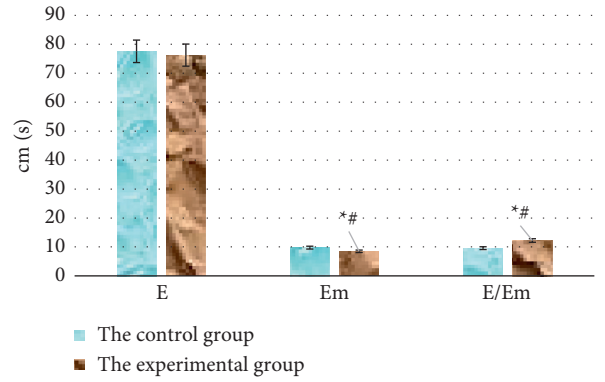

Figure 6: Comparison on (E) Em, and E/Em between the two groups of patients. ∗# means there was a significant difference ($P < 0.05$).

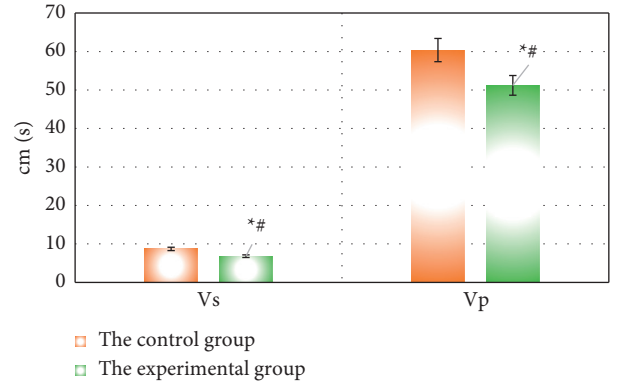

Figure 7: Comparison on Vs and Vp between the two groups of patients. ∗# means there was a significant difference ($P < 0.05$).

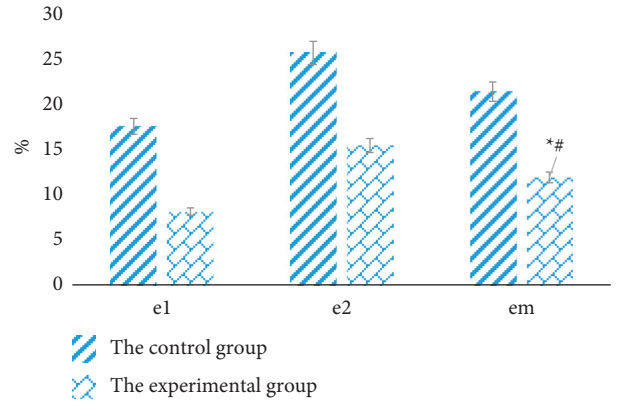

Figure 8: Comparison on the peak strain in the middle left atrium of the two groups of patients. ∗# means there was a significant difference ($P < 0.05$).

branch, which improves the robustness and reaches the advanced tracking level [18]. This also enables the combined use of the CNN model to more accurately and quickly classify and recognize ultrasound images.

Atrial fibrillation is the most common clinical arrhythmia, accounting for about 1/3 of all hospitalized patients with arrhythmia. In population studies, atrial fibrillation is most common in hypertension, ischemic heart disease, heart failure, and diabetes. Only <12% of patients with atrial fibrillation have no history of cardiopulmonary disease. The mortality rate is twice to that of patients with sinus rhythm and is related to the severity of the underlying disease [19]. In order to evaluate the effect of atrial fibrillation on the heart function of patients, this study excluded acute myocardial infarction, valvular heart disease, congenital heart disease, and other diseases that may affect heart function. In

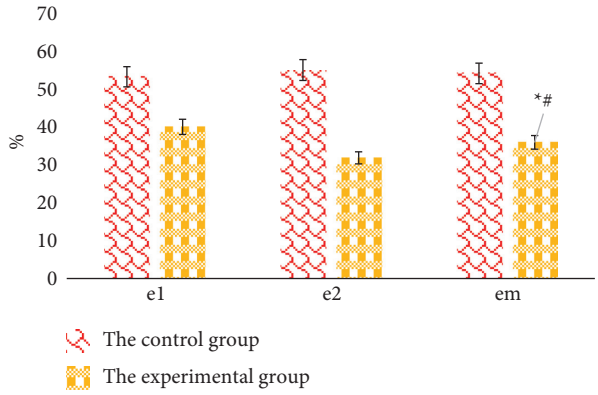

Figure 9: Comparison on the peak strain of the upper left atrium of the two groups of patients. *# means there was a significant difference ($P < 0.05$).

order to improve the image quality of cardiac ultrasound images, patients with advanced age, pulmonary heart disease, and thoracic deformities were excluded. Patients with no significant cardiac dilatation, normal left ventricular ejection fraction, no severe valvular disease, and similar factors such as ventricular rate and disease spectrum were selected as the control group.

Studies have confirmed that the occurrence of atrial fibrillation has a great relationship with the size of the left atrium, but the cause/effect is controversial. Atrial fibrillation ⟶ left atrium dilation ⟶ persistent atrial fibrillation ⟶ progressive left atrium dilatation, and enlargement of the left atrium is a risk factor for the occurrence of atrial fibrillation. Conventional cardiac ultrasound image parameters such as LAD, volume, and TA-EF have been widely used to assess the atrial structure and function of patients with atrial fibrillation. However, factors such as heart rate and front and rear load, will affect the accuracy of this parameter, so it cannot be directly used for the evaluation of atrial muscle movement [20]. Strain imaging combined with TNN is a new method that has emerged in recent years. It can represent the deformation of the local atrial segment without being affected by the load and other negative damages. It has excellent reproducibility and easy parameter measurement so as to provide accurate data for evaluating the contractility of the whole atrium and the segmental contraction in the long-axis direction and quantifying cardiac function [21]. Ijuin et al. [22] indicated that the strain peak was more stable and reproducible in the upper atrium, the peak gradually decreased from top to bottom, and the lower part was the same as the baseline, which was consistent with the results of this study. The Em measured in this article reflected the atrial storage function (the ability of the central atrial muscle to passively stretch during ventricular contraction). Compared with the control group, the Em value of the experimental group was lower, suggesting that atrial fibrillation may further damage the atrial muscle deformability. In this study, most patients in the experimental group had paroxysmal atrial fibrillation, and there may be no significant changes in the atrial structure, so there was no significant difference in LAD and volume between the experimental group and the control group. However, compared with the control group, the Em of the experimental group decreased, indicating that the traditional ultrasound structure test may not be able to assess the early effects of atrial fibrillation on left atrial function. The strain imaging combined with TNN to determine the strain peak of the left atrium can be used as a new method for more sensitive measurement of left atrial dysfunction in patients with atrial fibrillation.

Many heart failure trials have shown that an independent predictor of heart failure death and morbidity is atrial fibrillation, so the correct assessment of left ventricular function in patients with atrial fibrillation is very important. LVEF measurement is the most commonly used ultrasound measurement index for the quantitative evaluation of left ventricular systolic function. So far, it has been recognized that assessment of left ventricular diastolic and systolic function in patients with af is equally important [23]. Related literature reports that ventricular diastolic dysfunction is the cause of atrial fibrillation. Vp is a new indicator to evaluate left ventricular diastolic function. The change of preload has no effect on it but is related to the indoor pressure gradient during ventricular diastole. When the ventricular diastolic dysfunction is incapable of producing a large pressure gradient, it reduces or even disappears. Left ventricular diastolic function can be evaluated qualitatively and quantitatively by Vp, which has high sensitivity and specificity in the diagnosis of false normal [24]. TVI uses high frame rate synchronization processing technology, which can get a more accurate local myocardial velocity curve without being disturbed by atrial rhythm. Relevant studies have shown that the movement of myocardial fibers in a certain plane from the base to the apex can be called the movement of the mitral valve annulus, and there are a fewer myocardial fibers in any short-axis plane than in this plane. Therefore, the difference between normal and abnormal is magnified, and the dependence on local changes is less. The average velocity of the various parts of the mitral valve ring in the early diastole can be used as a sensitive indicator to reflect the left ventricular diastolic function, and it will hardly be disturbed by heart rate and load [25, 26]. The results of this study showed that the combined use of the TNN model can more accurately identify the Em, especially the E/Em value of patients with atrial fibrillation, which was greatly different from the control group, indicating that the left ventricular diastolic function measured by this method was more accurate.

5. Conclusion

In this study, the TNN model was combined with traditional ultrasound, Doppler spectrum, TVI, and strain imaging technology to classify and compare the relevant indicators of patients with cardiac atrial fibrillation, and detect indicators such as Vp, Em, E/Em, and Vs. It was found that this method was hardly disturbed by atrial contraction and heart rhythm, and the use of this model for atrial fibrillation patients can avoid the shortcomings of traditional detection methods and can more sensitively reflect the left ventricular contraction and diastolic function of the heart. The atrial muscle

deformation index strain peak velocity can prompt the left atrium dysfunction earlier than traditional detection techniques. The model had the advantages of rapidness and accuracy, and would play an important role in guiding the treatment and prognosis of patients with atrial fibrillation in the future. The simplification of the model and optimization of speckle tracking methods can further increase the processing speed and make it more practical in clinical practice. However, the confirmation of its conclusions still needed to be further supplemented and improved due to the small sample size of this study and the short tracking time.

Data Availability

The data used to support the findings of this study are available from the corresponding author upon request.

Conflicts of Interest

The authors declare no conflicts of interest.

Acknowledgments

This work was supported by Zhangjiakou Science and Technology Bureau Project (no. 2021087D).

References

[1] K. Karamchandani, A. K. Khanna, S. Bose, R. J. Fernando, and A. J. Walkey, "Atrial fibrillation," *Anesthesia & Analgesia*, vol. 130, no. 1, pp. 2–13, 2020.

[2] E. Achkasov, S. Bondarev, V. Smirnov et al., "Atrial fibrillation in athletes-features of development, current approaches to the treatment, and prevention of complications," *International Journal of Environmental Research and Public Health*, vol. 16, no. 24, p. 4890, 2019.

[3] C. E. E. d. Prazeres, T. A. Magalhães, A. C. de Castro Carneiro et al., "Image quality and radiation exposure Comparison of a double high-pitch acquisition for coronary computed tomography angiography versus standard retrospective spiral acquisition in patients with atrial fibrillation," *Journal of Computer Assisted Tomography*, vol. 42, no. 1, pp. 45–53, 2018.

[4] V. Ruddox, I. Sandven, J. Munkhaugen, J. Skattebu, T. Edvardsen, and J. E. Otterstad, "Atrial fibrillation and the risk for myocardial infarction, all-cause mortality and heart failure: a systematic review and meta-analysis," *European Journal of Preventive Cardiology*, vol. 24, no. 14, pp. 1555–1566, 2017.

[5] X. Zhang, H. Shen, and Z. Lv, "Deployment optimization of multi-stage investment portfolio service and hybrid intelligent algorithm under edge computing," *PLoS One*, vol. 16, no. 6, Article ID e0252244, 2021.

[6] S. A. Virk, R. G. Bennett, C. Chow et al., "Catheter ablation versus medical therapy for atrial fibrillation in patients with heart failure: a meta-analysis of randomised controlled trials," *Heart Lung & Circulation*, vol. 28, no. 5, pp. 707–718, 2019.

[7] Y. Ma, F. Bai, F. Qin et al., "Catheter ablation for treatment of patients with atrial fibrillation and heart failure: a meta-analysis of randomized controlled trials," *BMC Cardiovascular Disorders*, vol. 18, no. 1, p. 165, 2018.

[8] Z. U. A. Asad, A. Yousif, M. S. Khan, S. M. Al-Khatib, and S. Stavrakis, "Catheter ablation versus medical therapy for atrial fibrillation," *Circulation: Arrhythmia and Electrophysiology*, vol. 12, no. 9, Article ID e007414, 2019.

[9] M. Zhu, X. Zhou, H. Cai et al., "Catheter ablation versus medical rate control for persistent atrial fibrillation in patients with heart failure," *Medicine*, vol. 95, no. 30, p. e4377, 2016.

[10] A. AlTurki, R. Proietti, A. Dawas, H. Alturki, T. Huynh, and V. Essebag, "Catheter ablation for atrial fibrillation in heart failure with reduced ejection fraction: a systematic review and meta-analysis of randomized controlled trials," *BMC Cardiovascular Disorders*, vol. 19, no. 1, p. 18, 2019.

[11] L. P. Badano, T. J. Kolias, D. Muraru et al., "Standardization of left atrial, right ventricular, and right atrial deformation imaging using two-dimensional speckle tracking echocardiography: a consensus document of the EACVI/ASE/Industry Task Force to standardize deformation imaging," *European Heart Journal - Cardiovascular Imaging*, vol. 19, no. 6, pp. 591–600, 2018.

[12] A. A. Leroux, M. Moonen, F. Farnir, S. Deleuze, C. Sandersen, and H. Amory, "Two-dimensional speckle tracking echocardiography in goats: repeatability, variability, and validation of the technique using an exercise test and an experimentally induced acute ischemic cardiomyopathy," *BMC Veterinary Research*, vol. 16, no. 1, p. 56, 2020.

[13] Z. Lv, D. Chen, B. Cao, H. Song, and H. Lv, "Secure deep learning in defense in deep-learning-as-a-service computing systems in digital twins," *IEEE Transactions on Computers*, vol. 26, 2021.

[14] D. F. Briceño, T. M. Markman, F. Lupercio et al., "Catheter ablation versus conventional treatment of atrial fibrillation in patients with heart failure with reduced ejection fraction: a systematic review and meta-analysis of randomized controlled trials," *Journal of Interventional Cardiac Electrophysiology*, vol. 53, no. 1, pp. 19–29, 2018.

[15] Z. Wan, Y. Dong, Z. Yu, H. Lv, and Z. Lv, "Semi-supervised support vector machine for digital twins based brain image fusion," *Frontiers in Neuroscience*, vol. 15, Article ID 705323, 2021.

[16] X. Zhu, Y. Wei, Y. Lu et al., "Comparative analysis of active contour and convolutional neural network in rapid left-ventricle volume quantification using echocardiographic imaging," *Computer Methods and Programs in Biomedicine*, vol. 199, Article ID 105914, 2021.

[17] X. Lv, S. Wang, and D. Ye, "CFNet: LiDAR-camera registration using calibration flow network," *Sensors*, vol. 21, no. 23, p. 8112, 2021.

[18] C. Li, Q. Xing, and Z. Ma, "HKSiamFC: visual-tracking framework using prior information provided by staple and kalman filter," *Sensors*, vol. 20, no. 7, p. 2137, 2020.

[19] P. Mazzone, P. Della Bella, and A. Radinovic, "Left atrial appendage occlusion in patients with atrial fibrillation and a large prevalence of intracranial bleeding: a further confirmation," *Journal of Cardiovascular Medicine*, vol. 21, no. 8, pp. 592–594, 2020.

[20] M. Sangsriwong, G. Cismaru, M. Puiu et al., "Formula to estimate left atrial volume using antero-posterior diameter in patients with catheter ablation of atrial fibrillation," *Medicine*, vol. 100, no. 29, Article ID e26513, 2021.

[21] G. Abdelmohsen, H. Mohamed, M. Mohsen et al., "Evaluation of cardiac function in pediatric patients with mild to moderate bronchial asthma in the era of cardiac strain imaging," *Pediatric Pulmonology*, vol. 54, no. 12, pp. 1905–1913, 2019.

[22] S. Ijuin, A. Hamadanchi, F. Haertel et al., "Improvement in left atrial strain among patients undergoing percutaneous left

atrial appendage closure," *Journal of Cardiovascular Echography*, vol. 30, no. 1, pp. 15–21, 2020.

[23] K.-H. Kuck, B. Merkely, R. Zahn et al., "Catheter ablation versus best medical therapy in patients with persistent atrial fibrillation and congestive heart failure," *Circulation: Arrhythmia and Electrophysiology*, vol. 12, no. 12, Article ID e007731, 2019.

[24] W. Shi, H. X. Liu, Z. D. Xuan, L. Zhao, J. Z. Li, and Y. H. Wang, "Assessments of M-mode color cardiac ultrasound images on fetal right ventricular diastolic function with umbilical cord around neck," *European Review for Medical and Pharmacological Sciences*, vol. 21, no. 12, pp. 2927–2933, 2017.

[25] H. Kim, I. C. Kim, S. W. Choi, J. W. Chung, and J. Y. Kim, "Clinical significance of early-diastolic tissue velocity imaging of lateral mitral annulus for prognosis of nonischemic left ventricular dysfunction," *Journal of Clinical Ultrasound*, vol. 48, no. 3, pp. 160–167, 2020.

[26] S. Futami, J. Ishikawa, T. Maeda, M. Kawano, C. Sakurayama, and K. Harada, "Factors contributing to energy loss in left ventricle during diastolic and systolic phases in elderly patients," *Echocardiography*, vol. 38, no. 1, pp. 72–80, 2021.